

## Article

# Preparation of Gallic Acid Intercalated Layered Double Hydroxide for Enhanced Corrosion Protection of Epoxy Coatings

Shuo Fang<sup>1,2</sup>, Kaifeng Chen<sup>2</sup>, Hongrui Yao<sup>1</sup>, Yanhui Cao<sup>2</sup> , Shuli Guo<sup>3</sup>, Li Wang<sup>3</sup>, Yangsong Wang<sup>4</sup>, Shuai Yu<sup>4</sup> and Na Wang<sup>1,\*</sup>

<sup>1</sup> Liaoning Provincial Key Laboratory for Synthesis and Preparation of Special Functional Materials, Shenyang University of Chemical Technology, Shenyang 110142, China

<sup>2</sup> State Key Laboratory for Marine Corrosion and Protection, Luoyang Ship Material Research Institute (LSMRI), Xiamen 361101, China

<sup>3</sup> Shenyang Research Institute of Industrial Technology for Advanced Coating Materials, Shenyang 110300, China

<sup>4</sup> Liaoning Shunfeng New Material Technology Co., Ltd., Shenyang 110326, China

\* Correspondence: iamwangna@syuct.edu.cn; Tel.: +86-13840257976

**Abstract:** In the field of corrosion protection coatings, layered double hydroxide (LDH) has gained wide attention as a novel controlled-release nanocontainer. In this paper, by using a co-precipitation to store corrosion inhibitors in layered double hydroxide with barrier properties, an environmentally friendly gallic acid (GA) intercalated layered double hydroxide corrosion protection filler (GA-LDH) was prepared. The epoxy coating was then modified with GA-LDH to improve its corrosion protection performance. The structure, composition, and release behavior of GA-LDH were investigated by a series of characterizations, such as field emission scanning electron microscopy (FE-SEM), X-ray diffraction (XRD), Fourier transform infrared spectroscopy (FT-IR) and ultraviolet-visible spectrophotometry (UV-vis). Electrochemical impedance spectroscopy (EIS) and a neutral salt spray test (NSS) were performed to evaluate the effect of EP coating containing GA-LDH on corrosion protection for Q235 steel. The results show that GA-LDH added to an epoxy coating can achieve excellent corrosion protection performance and is expected to be widely used in marine corrosion protection contexts.

**Keywords:** layered double hydroxide; gallic acid; epoxy coating; corrosion protection



**Citation:** Fang, S.; Chen, K.; Yao, H.; Cao, Y.; Guo, S.; Wang, L.; Wang, Y.; Yu, S.; Wang, N. Preparation of Gallic Acid Intercalated Layered Double Hydroxide for Enhanced Corrosion Protection of Epoxy Coatings. *Coatings* **2023**, *13*, 128. <https://doi.org/10.3390/coatings13010128>

Academic Editors: Nicolas Mary and Véronique Vitry

Received: 9 December 2022

Revised: 27 December 2022

Accepted: 2 January 2023

Published: 10 January 2023



**Copyright:** © 2023 by the authors. Licensee MDPI, Basel, Switzerland. This article is an open access article distributed under the terms and conditions of the Creative Commons Attribution (CC BY) license (<https://creativecommons.org/licenses/by/4.0/>).

## 1. Introduction

Metal is inevitably corroded in the marine environment, which will not only cause substantial economic losses, but the structural damage caused by corrosion will bring more severe safety problems [1,2]. Therefore, it is essential to improve corrosion protection performance to prevent or slow down the corrosion of metal [3]. The application of corrosion protection coatings to avoid direct exposure of the metal substrate surface to corrosive media is, up to present, the most common way to protect metallic materials [4]. Epoxy resin has excellent adhesion, good mechanical properties, thermal stability and is widely used for corrosion protection coatings [5,6]. Nevertheless, the curing of epoxy resin is done during the evaporation of the solvent, which can leave the generation of micropores and cracks that cause corrosive media to enter the coating and shorten its life [7,8]. To solve this problem, fillers such as two-dimensional layered materials [9], MOFs [10], silicates [11], and phosphates [12] have received increasing attention. Among them, the incorporation of nanomaterials with two-dimensional structure is a good choice. Their high aspect ratio will prolong the diffusion path of the corrosive medium in the coating and may delay the coating failure [13].

Layered double hydroxide (LDH) is a unique structure of two-dimensional material, also commonly referred to as a hydrotalcite-like compound. The molecular formula of LDH is usually denoted by  $[M_{1-x}^{2+}M_x^{3+}(\text{OH})_2]^{x+}[A_{x/n}^{n-}] \cdot m\text{H}_2\text{O}$ , where  $M^{2+}$  and  $M^{3+}$  are the metal cations of mixed metal hydroxide layers, and  $A^{n-}$  is an anion present in the interlayer channel.  $A^{n-}$  is loosely bound to the main layer structure by electrostatic interaction, so it can perform exchange reactions with other anions [14,15]. Thus, layered double hydroxide serves as a typical nanocontainer that can encapsulate organic or inorganic corrosion inhibitors. Corrosive anions are captured, and interlayer corrosion-inhibiting anions are released through exchange reactions, thus providing corrosion protection [16]. For example, Na Wang et al. [17] synthesized tripolyphosphate intercalated LDHs by a co-precipitation method to modify waterborne epoxy resin. In both EIS and salt spray test results, for the performance of STPP-LDHs composite coating with each addition the ratio was much better than pure EP coating. Ang Liu et al. [18] used the ion exchange method and the exfoliation and reassembly to incorporate 5-methyl-1,3,4-thiadiazole-2-thiol (MTT) into LDH, respectively. It was shown that the exfoliation and reassembly had about four times higher loading capacity than the anion-exchange method. Moreover, more MMT would be released during protection, improving the corrosion inhibition efficiency by about 30%. E. Alibakhshi et al. [19] successfully inserted  $\text{PO}_4^{3-}$  into Mg-Al LDH by anion exchange. Their experiment verified that Mg-Al- $\text{PO}_4^{3-}$  released  $\text{PO}_4^{3-}$  during the dissolution of LDH support, which formed an inhibitory film on the mild steel surface. It showed a significant corrosion inhibition effect and effectively improved the adhesion strength to mild steel. However, since the organic and inorganic corrosion inhibitors produced are often harmful, research on environmentally friendly corrosion inhibitors to replace conventional ones is attracting increasing interest.

Gallic acid (GA), a green corrosion inhibitor, is inexpensive, renewable, and widely found in various plants [20–22]. Previous studies have shown that GA is often used as an essential component of rust converters [23,24]. In the structure of GA, the two neighboring phenolic hydroxyl groups on the benzene ring have a strong chelating ability that can form stable bidentate chelates with  $\text{Fe}^{2+}$  and  $\text{Fe}^{3+}$ , which will retard the corrosion reaction of the cathode [25]. However, GA has a strong water absorption and will inevitably damage the coating performance when added to the coating. If one wants to apply GA to the coating, storing it in a container will be a better method.

Inspired by the above considerations, a one-step preparation of gallic acid (GA) intercalated layered double hydroxide (LDH) green corrosion protection filler (GA-LDH) was carried out by a co-precipitation method. On the basis of improving the denseness of the epoxy coating, the green corrosion inhibitor is released through the absorption of chloride ions by the nano-container. It can chelate with metal ions and form a shielding layer on the surface of the substrate to achieve enhanced corrosion protection of the epoxy coating. Potentially harmful effects of nanoparticles on the environment and coatings are effectively avoided.

## 2. Experimental

### 2.1. Materials

Gallic acid (99.0%, Macklin, Shanghai, China) ( $\text{C}_7\text{H}_6\text{O}_5$ , GA), zinc nitrate hexahydrate (99.0%, SCR, Shanghai, China) ( $\text{Zn}(\text{NO}_3)_2 \cdot 6\text{H}_2\text{O}$ ), aluminum nitrate nonahydrate (99.0%, McLean) ( $\text{Al}(\text{NO}_3)_3 \cdot 9\text{H}_2\text{O}$ ), sodium hydroxide (96.0%, SCR) (NaOH), ethanol (99.7%, SCR) (EtOH), and sodium chloride (99.5%, SCR) (NaCl) were all purchased chemicals and solvents and can be used directly without purification.

The following were also obtained: epoxy resin (6101, Sinopec, Yueyang, China) ( $(\text{C}_{11}\text{H}_{12}\text{O}_3)_n$ , EP), xylene (99.50%, Sinopec), n-butanol (99.90%, Sinopec), dispersing agent (BYK-110, BYK-CHEMIE), leveling agent (BYK-320, BYK-CHEMIE, Tongling, China), defoamer (BYK-530, BYK-CHEMIE), phenolic amine hardener (Nx2015, Cardolite, Zhuhai, China), Q235 plate (150 mm × 70 mm × 2 mm, Xiamen Qianfeng Machinery Co., Xiamen, China).

## 2.2. The Synthesis of LDH and GA-LDH

GA-LDH was synthesized by using a co-precipitation method [26,27]. 0.01 mol GA was dissolved in 50 mL of mixed solution (1:1 ethanol to deionized water by volume), and the pH was adjusted to approximately 10 by using a 1 M NaOH solution. Under a nitrogen flow with magnetic stirring, 50 mL of aqueous solutions of 0.02 mol  $Zn(NO_3)_2 \cdot 6H_2O$  and 0.01 mol  $Al(NO_3)_3 \cdot 9H_2O$  were added dropwise while maintaining the pH with 1 M NaOH solution. The precipitates were aged at ambient temperature for 24 h, then centrifuged and washed with deionized water. The target product GA-LDH was finally obtained by freeze-drying, and its structure schematic diagram is shown in Figure 1b.

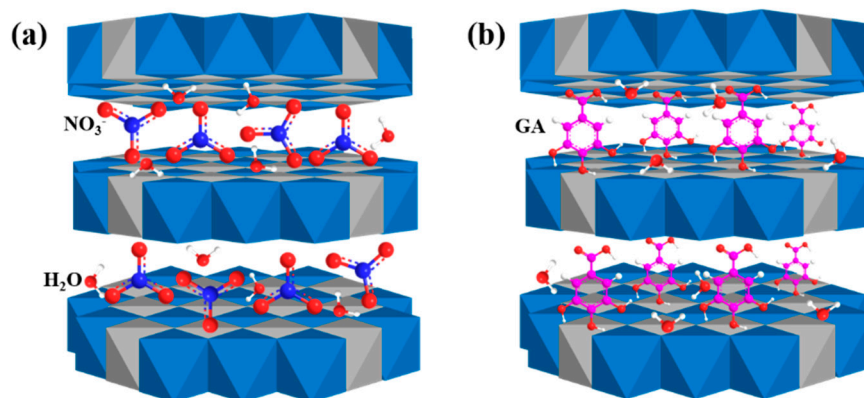


**Figure 1.** Schematic diagrams of the structure of (a) LDH and (b) GA-LDH.

Zinc-aluminum LDH (Figure 1a) was synthesized in the same way without GA [28]. Under a nitrogen flow, 1 M NaOH solution was slowly added to the aqueous solution of  $Zn(NO_3)_2 \cdot 6H_2O$  and  $Al(NO_3)_3 \cdot 9H_2O$  mixed under the same conditions as above until the pH was about 10. Next, the solutions was aged at ambient temperature for 24 h, and then centrifuged and washed with deionized water, and freeze-dried for use.

## 2.3. Preparation of Protective Coatings

A certain proportion of LDH and GA-LDH (1 wt.%) was added to 3 g diluent (7:3 volume ratio of xylene to n-butanol) and ultra-sonic treatment was performed for 30 min [29]. Then 16 g epoxy resin 6101 was added, along with 1 wt.% BYK-110 dispersing agent, BYK-320 leveling agent, and BYK-530 defoaming agent, and stirred for 10 min [30]. Subsequently, 10.56 g phenolic amine hardener Nx2015 (66 wt.% 6101) was added and stirred for 10 min. The coatings were uniformly brushed onto Q235 steel with a small brush and cured at ambient temperature for 72 h and named LDH/EP and GA-LDH/EP, respectively. Meanwhile, pure EP coating was prepared for comparison according to the above procedure.

## 2.4. Characterization

The morphology of the samples was observed by field emission scanning electron microscopy (FE-SEM, ZEISS 112 ULTRA55, Dresden, Germany) and high-resolution transmission electron microscopy (HR-TEM, JEM-2100F, JEOL, Tokyo, Japan). The structure was characterized by X-ray diffraction (XRD, XPERT-PRO, Almelo, The Netherlands) with Cu  $K\alpha$  radiation ( $\lambda = 0.154$  nm) at 40 kV and 40 mA. The chemical composition of the samples was confirmed by using X-ray energy spectrometry (EDS, Oxford, UK) and Fourier transform infrared spectroscopy (FT-IR, Nexus 670, Madison, WI, USA). An X-ray photoelectron spectrometer (XPS, PHI 5000 Versaprobe III, Chigasaki, Japan) was used to test the surface elemental state of the samples. The mass loss changes of the samples at 30 to 800 °C were analyzed by a thermogravimetric analyzer (TG-DTG, Rigaku TG/DTA8122, Tokyo, Japan) with a temperature rise rate of 10 °C/min. The controlled release of GA-LDH was investigated by using an Ultraviolet-visible spectrophotometer (UV-vis, Cary 5000, Agilent, Kuala Lumpur, Malaysia) at the wavelength  $\lambda_{max} = 269$  nm. Next, 1 g GA-LDH was added

to a 100 mL NaCl solution at a concentration of 3.5 wt.%, and the absorbance was measured by taking a trace amount of liquid at a predetermined time. The release concentration can be obtained from the equation of the calibration curve. The following calibration curve equation was used:  $y = 5.181 \times 10^{-2}x - 3.358 \times 10^{-2}$ ,  $R^2 = 0.99993$ , where  $x$  represents the GA concentration and  $y$  represents the absorbance in  $\mu\text{g/mL}$ .

An AC impedance tester (CS353, CorrTest, Wuhan, China) was used to perform electrochemical impedance spectroscopy (EIS) tests in a standard three-electrode system. The system consists of an Ag/AgCl reference electrode, a platinum sheet counter electrode, and a mild steel plate as the working electrode. Samples immersed in 3.5 wt.% NaCl solution for 7, 14, 21, 28, and 35 days were measured at 100 kHz to 0.01 Hz by using 10 mV AC amplitude over an area of  $7.065 \text{ cm}^2$  exposed to the working electrode. The neutral salt spray test (NSS) was carried out concerning the GB/T10125-2012 standard to research the corrosion protection of the samples in harsh environments. The length of manual scratches on the coated samples was about 5 cm. The coatings were photographed and recorded at 1, 2, 6, 10 and 14 d (days), respectively. For obtaining valid experimental data, three parallel samples of each coating were used in EIS and NSS tests.

### 3. Results and Discussion

#### 3.1. Characterization of GA-LDH

For LDH and GA-LDH prepared by the co-precipitation method in this study, the compositions and structures were characterized by various testing means. The microstructure and morphology of LDH and GA-LDH were visualized by using FE-SEM and HR-TEM, as shown in Figure 2. It was evident from the FE-SEM images that both prepared samples had inhomogeneous crystal morphology, showing different degrees of agglomeration and differed significantly from each other in terms of surface morphology. LDH exhibited an irregular lamellar structure and the presence of particles of different sizes, which was probably caused by the effect of pH on crystal nucleation and the incomplete growth of the crystals [31]. The GA-LDH sample also showed a lamellar structure with the typical characteristics of hydrotalcite-like structure, but with a relatively rougher surface. The reason for this feature may be the adsorption of gallic acid on the crystal surface [32]. As shown in Figure 2c,f, the HR-TEM images also show the lamellar structure of both samples with aggregation, and the curled edges of LDH can be seen. The EDS results of the samples in Figure 3 agreed with expectations, with the ratio of Zn and Al atoms in both samples close to two. The LDH contained 23.62% C and 8.94% N. The presence of N elements can be attributed to  $\text{NO}_3^-$ . In addition, the appearance of C may be due to surface contamination of the sample and  $\text{CO}_3^{2-}$  which had a relatively strong affinity for LDH [33]. It is noteworthy that the GA-LDH samples contained high contents of C, which revealed the successful loading of gallic acid.

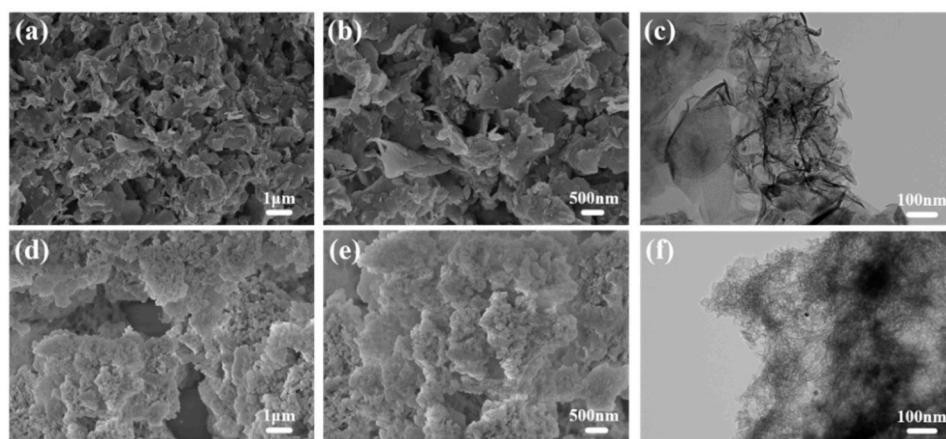


**Figure 2.** (a,b) FE-SEM images and (c) HR-TEM image of LDH; (d,e) FE-SEM images and (f) HR-TEM image of GA-LDH.

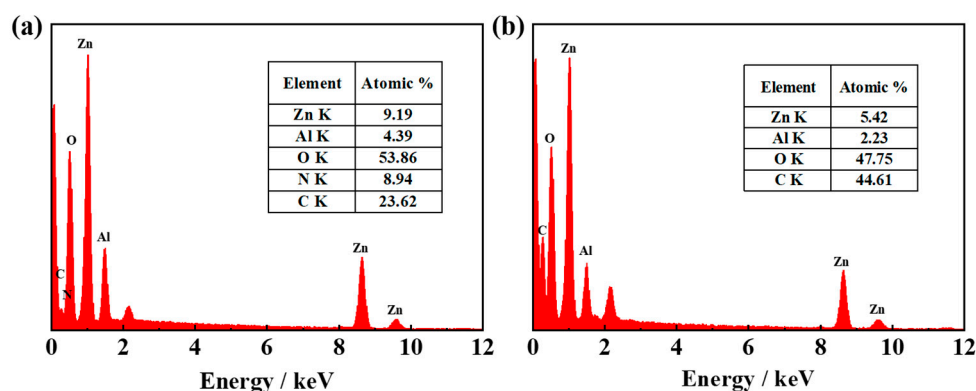


Figure 3. EDS results of (a) LDH and (b) GA-LDH.

Figure 4 shows the XRD patterns of LDH and GA-LDH. The LDH presented intense and symmetric diffraction peaks at  $10.03^\circ$ ,  $19.93^\circ$ ,  $33.80^\circ$  and  $60.34^\circ$ , corresponding to the reflections of (003), (006), (009) and (110), respectively. The layer spacing in the (003) plane was calculated to be 0.88 nm by using the Bragg equation, indicating the existence of nitrate anions between the layers of LDH [34,35]. The typical characteristic diffraction peaks in LDH were also observed in the GA-LDH curve. The  $2\theta$  value of the (003) diffraction peak was  $7.01^\circ$ , so the layer spacing was 1.26 nm. Compared with LDH, the (003) diffraction peak of GA-LDH shifted to a lower diffraction angle and the layer spacing increased, which implies that GA successfully intercalated into the layers of LDH.

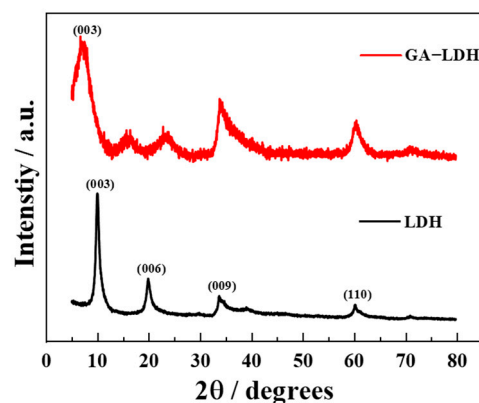


Figure 4. XRD patterns of LDH and GA-LDH.

The FT-IR spectra (Figure 5) were utilized to further characterize the functional groups of LDH and GA-LDH. For the FTIR spectra of LDH, the relatively broad peak around  $3450\text{ cm}^{-1}$  was caused by the stretching vibration of  $-\text{OH}$  on the LDH surface and hydroxyl groups of interlayer water molecules, and  $1646\text{ cm}^{-1}$  was the deformation vibration of interlayer water molecules [36,37]. The absorption peak at  $1361\text{ cm}^{-1}$  and a higher wave number shoulder peak were observed corresponding to  $\text{NO}_3^-$  and  $\text{CO}_3^{2-}$  impurities, respectively [38]. The FT-IR spectra of GA-LDH also showed the same characteristic group absorption peaks of hydrotalcite-like groups. The characteristic peaks at  $1220\text{ cm}^{-1}$  and  $1367\text{ cm}^{-1}$  were associated with carboxyl groups [39]. In addition,  $1521\text{ cm}^{-1}$  and  $752\text{ cm}^{-1}$  were due to benzene ring backbone vibrations, and  $1092\text{ cm}^{-1}$  was attributed to aromatic ring C-H deformation [40,41]. The presence of carboxyl and benzene ring characteristic absorption peaks in the gallic acid structure was a piece of strong evidence for the presence of GA.

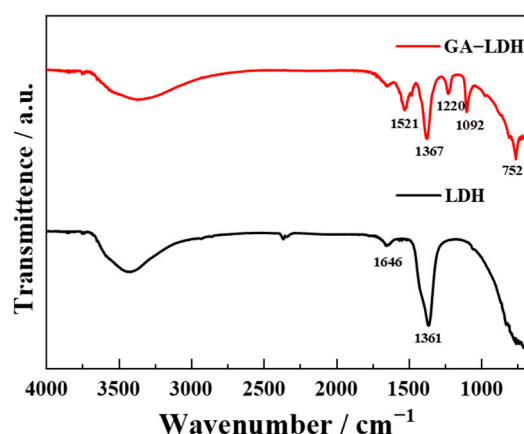


Figure 5. FT-IR spectra of LDH and GA-LDH.

To better analyze the chemical states of the elements in LDH and GA-LDH, the characterization was carried out by XPS. Figure 6a shows the XPS full spectra of LDH and GA-LDH both contain Zn, Al, C and O. However, the difference was that GA-LDH lacked N relative to LDH, meaning the interlayer anion of GA-LDH was not the nitrate anion. In addition, the C 1s and O 1s of both samples were analyzed using high-resolution XPS spectra. For LDH, the C 1s (Figure 6b) has two peaks, including the abnormal carbon at 284.8 eV and the O-C=O group associated with  $\text{CO}_3^{2-}$  at 288.91 eV [42]. The O 1s of LDH (Figure 6c) was classified as 530.37 eV, 531.02 eV, and 531.69 eV, and is attributed to M-O, C=O and adsorbed water molecules, respectively [43]. The C 1s of GA-LDH (Figure 6d) has three peaks, the binding energy at 284.8 eV was mainly associated with C-C/C=C and 288.65 eV was attributed to the carboxylate O-C=O [39]. In addition, 285.27 eV corresponded to the C-OH of the phenolic hydroxyl group [41,44]. Furthermore, the O 1s (Figure 6e) were fitted as three curves, M-O (530.86 eV), C-OH (531.42 eV), and O-C=O (532.38 eV), respectively. Thus, the XPS full spectra indicate that LDH was mainly intercalated with nitrate anion. Combined with the analysis of GA-LDH high-resolution XPS spectra, successful GA loading was likewise demonstrated.

The thermal decomposition processes of LDH and GA-LDH were investigated by TG-DTG curves. The curve of LDH is shown in Figure 7a, and the process underwent four mass losses. The first mass loss occurred at 30 to 120 °C, which was ascribed to the removal of physisorbed water molecules. The second mass loss occurred at 120 to 170 °C which was probably related to the elimination of water molecules between the LDH layers. The third mass loss occurred at 170 to 280 °C, and the corresponding DTG curve showed a shoulder peak at 213 °C, indicating that the two processes may have occurred concurrently over this temperature range. This phenomenon was thought to be the dehydroxylation of hydrotalcite-like sheets and the decomposition of a small number of interlayer carbonate anions [45,46]. The fourth mass loss occurred at 280 to 510 °C, and the peak of the DTG curve in this range appeared at 371 °C, indicating that it may be due to the decomposition of nitrate [47]. For the thermal degradation curve of GA-LDH (Figure 7b), the cause of mass loss occurring at 30 to 170 °C was the same as that of LDH. However, GA-LDH lost more weight than LDH in this temperature range, which may be the result of GA water absorption. The second mass loss caused by dehydroxylation occurred at 170 to 300 °C. The third mass loss was at 300 to 480 °C, which was thought to be the decomposition of the GA between the layers [48]. The fourth mass loss occurred at 480 to 620 °C, and it was related to the collapse of the hydrotalcite-like layers [49].

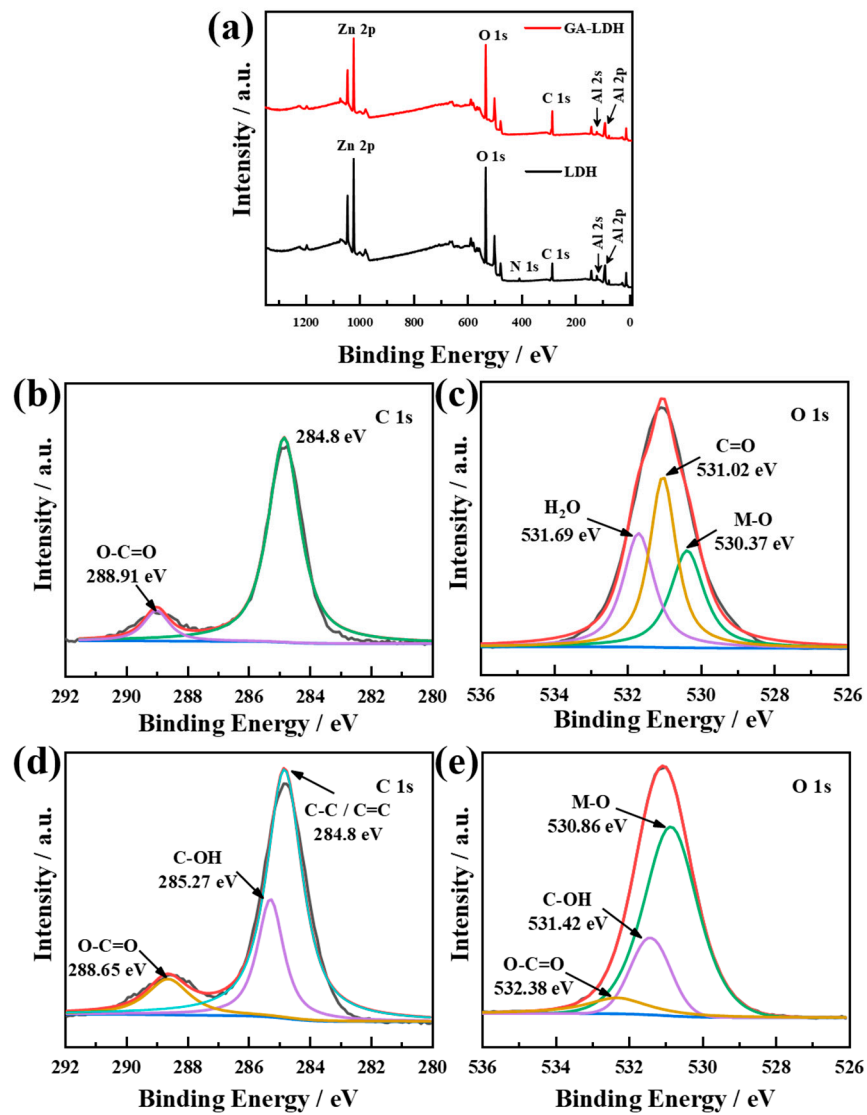


Figure 6. XPS spectra of (a) LDH and GA-LDH. High-resolution XPS spectra of LDH (b) C 1s, (c) O 1s and GA-LDH (d) C 1s, (e) O 1s.

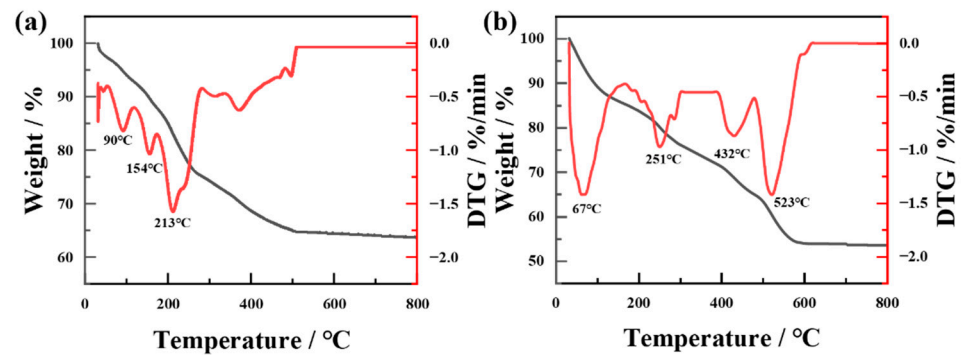
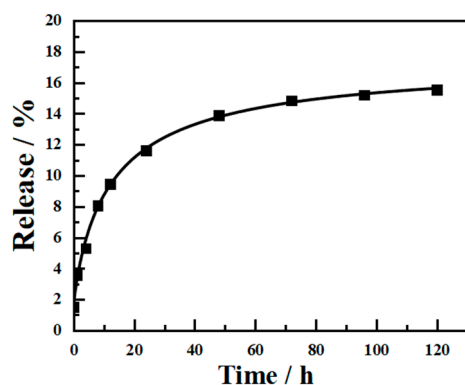


Figure 7. TG–DTG curves of (a) LDH and (b) GA–LDH.

UV-vis spectroscopy measured the concentration of components released from GA-LDH at predetermined times in a 3.5 wt.% NaCl solution. The release curve in Figure 8 shows that the release of gallate anion increases with time. The whole release process in general can be summarized in two phases. First, the gallate anion release tended to

increase rapidly during the initial 24 h, with a release rate of about 11.6%. The trend of increase then slowed down. The whole measurement process lasted 120 h and released a total of about 15.5%. This result confirms the anion exchange ability of GA-LDH and indicates that the anion exchange of gallate anion was a slow and persistent process. The phenomenon of slow release of the gallate anion may be caused by the decreasing chloride ion concentration of the ion exchange reaction with the reaction and the stronger interaction between the hydroxyl group of GA and the substrate [40].



**Figure 8.** Release curve of gallate anion in 3.5 wt.% NaCl solution.

### 3.2. Characterization of Coatings Corrosion Protection Performance

The corrosion behavior of the prepared pure EP, LDH/EP, and GA-LDH/EP coatings was explored by EIS. Figure 9 shows the Nyquist and Bode Phase plots for all coatings after being soaked at different times. The scatter points in the figure were the raw data and the solid line data were obtained by the equivalent circuit fitting in Figure 10.

Figure 9a,c,e show the results of impedance tests expressed as Nyquist curves. After the pure EP coating was immersed for 7 days, two time constants appeared in the Nyquist curve, which implies that the corrosive medium came into contact with the substrate via the micropores left by curing and that corrosion occurred [50]. The presence of Warburg impedance in the low-frequency region of the Nyquist curve suggests that corrosion was controlled by a change from the charge transfer to diffusion processes. As the immersion time of the coating increased, more defects appeared in the coating, resulting in a rapid decrease in the impedance arc radius. For the LDH/EP coating, the second time constant appeared later, and the impedance arc radius was larger, which reflected the good barrier effect of the hydrotalcite-like structure in the EP coating. However, it is remarkable that the radius of the circle of the Nyquist curve for the GA-LDH/EP was considerably larger than the other two control coatings, which represents a better impedance behavior, and is visually reflected in the effect of gallic acid intercalation.

The low-frequency impedance mode values can reflect the ease of ion passage through the coating [51]. The Bode plot results show a rapid drop of  $|Z|_{0.01 \text{ Hz}}$  from  $6.37 \times 10^7 \Omega \text{ cm}^2$  to  $5.69 \times 10^5 \Omega \text{ cm}^2$  after 35 days of immersion in the pure EP coating. The situation may be that a large amount of corrosion medium infiltration accelerates the electrochemical reaction that occurs at the interface. For LDH/EP, the  $|Z|_{0.01 \text{ Hz}}$  for 35d was  $4.78 \times 10^6 \Omega \text{ cm}^2$ , which is an order of magnitude higher than that of the pure EP coating in the end. This was a result of the addition of LDH nanosheets. LDH nanosheets made up for some of the deficiencies, and corrosive media were more difficult to penetrate the coating. However, the  $|Z|_{0.01 \text{ Hz}}$  of the coating with GA-LDH nanosheets added reached  $4.52 \times 10^9 \text{ cm}^2$  after 7 days of immersion and dropped to  $5.88 \times 10^8 \text{ cm}^2$  after 21 days. However, the decrease in the low-frequency impedance modulus became slow after 21 days. This was attributed to the generation of a chelate shield at the interface of the coating substrate by the released gallate anions, which hindered corrosion expansion [52]. Moreover, the superiority of GA-LDH corrosion protection was reflected by the wider frequency range of the maximum phase angle of GA-LDH/EP. The above results show that the improved

corrosion protection performance of GA-LDH was not only generated by the “labyrinth effect” of the lamellar structure but also because of the positive effect of the gallate anion released from the nanocontainer to chelate the metal ions to form a stable shielding layer.

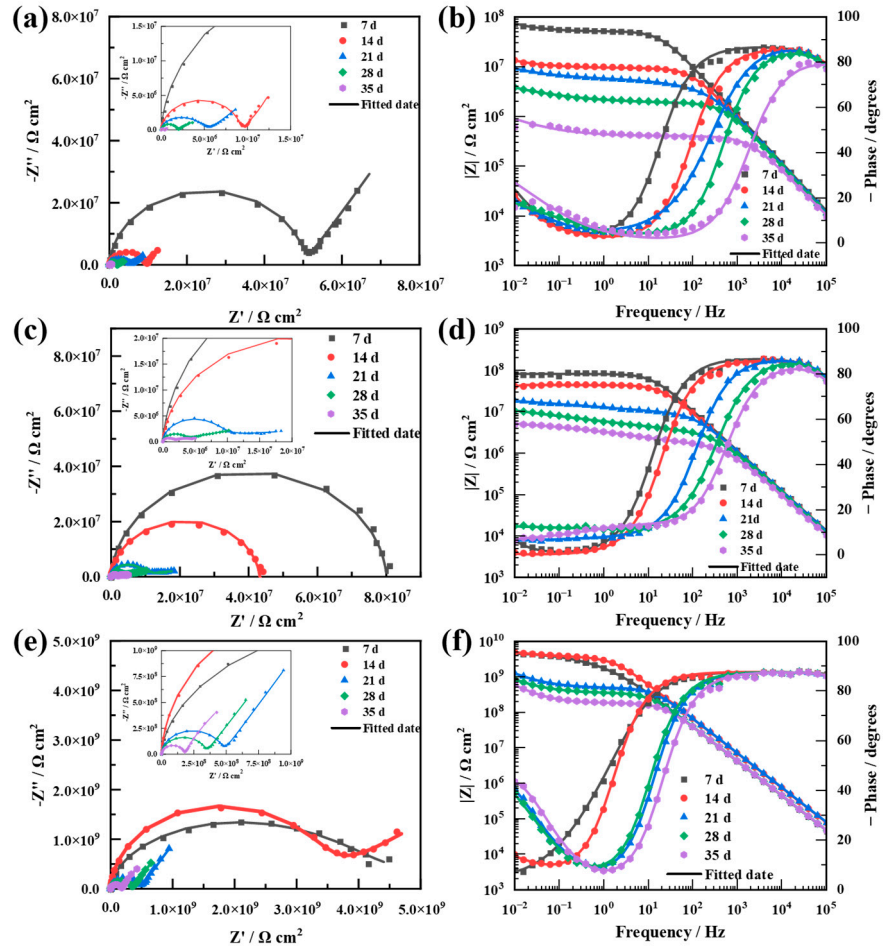


**Figure 9.** (a,c,e) Nyquist and (b,d,f) Bode plots of (a,b) pure EP; (c,d) LDH/EP; and (e,f) GA–LDH/EP coatings coated on Q235 steel.(The insets in (a,c,e) are Nyquist plots of the respective magnified high-frequency regions.).

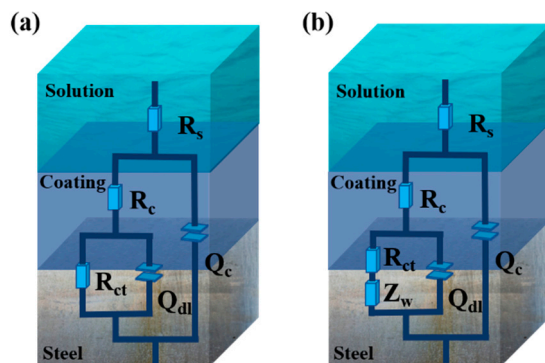


**Figure 10.** Schematic diagram of the equivalent circuit used to fit the EIS data. (a) diffusion of the corrosive medium to the coating-substrate interface; (b) with Warburg impedance.

The raw experimental information was fitted by way of the equivalent circuit shown in Figure 10, where  $R_s$  is the solution resistance,  $R_c$  and  $Q_c$  are the coating resistance and capacitance,  $R_{ct}$  and  $Q_{dl}$  represent the charge-transfer resistance and double layer capacitance and  $Z_w$  is the Warburg impedance [53]. When the coating was immersed for a

while, the corrosion medium began to diffuse to the coating-substrate interface, and the equivalent circuit diagram at this point is shown in Figure 10a. If the impedance spectrum contains Warburg impedance, and the circuit diagram of Figure 10b is chosen. Table 1 shows the relevant parameters fitted by the equivalent circuit. Comparing all coatings, it is obvious that the GA-LDH/EP coating had the highest  $R_c$  and  $R_{ct}$  values.  $R_c$  can indicate the denseness of the coating, and it is critical data for judging the corrosion protection performance of the coating. Therefore, this result reflects that GA-LDH added to the coating can reduce the number of defects and protect the substrate with remarkable effects.

**Table 1.** Values of electrochemical corrosion parameters obtained by fitting EIS data.

Coating	Time (d)	$R_c$ ( $\Omega \cdot \text{cm}^2$ )	$Q_c$ ( $\text{F} \cdot \text{cm}^{-2}$ )	$n_c$	$R_{ct}$ ( $\Omega \cdot \text{cm}^2$ )	$Q_{dl}$ ( $\text{F} \cdot \text{cm}^{-2}$ )	$n_{dl}$	$Z_w$ ( $\Omega \cdot \text{cm}^2$ )
Pure EP	7	$5.04 \times 10^7$	$1.96 \times 10^{-10}$	0.97	$1.08 \times 10^6$	$1.66 \times 10^{-8}$	0.60	$1.30 \times 10^{-7}$
	14	$7.49 \times 10^6$	$2.06 \times 10^{-10}$	0.98	$1.64 \times 10^6$	$1.45 \times 10^{-7}$	0.95	$7.60 \times 10^{-7}$
	21	$4.87 \times 10^6$	$3.46 \times 10^{-10}$	0.93	$1.53 \times 10^6$	$6.87 \times 10^{-7}$	0.40	$9.43 \times 10^{-7}$
	28	$1.83 \times 10^6$	$2.30 \times 10^{-10}$	0.97	$1.39 \times 10^6$	$1.28 \times 10^{-6}$	0.36	$1.75 \times 10^{-6}$
	35	$3.77 \times 10^5$	$4.38 \times 10^{-10}$	0.94	$1.03 \times 10^6$	$5.18 \times 10^{-6}$	0.39	$3.81 \times 10^{-5}$
LDH/EP	7	$8.20 \times 10^7$	$1.65 \times 10^{-10}$	0.98	$7.58 \times 10^7$	$1.18 \times 10^{-10}$	0.61	
	14	$4.31 \times 10^7$	$1.89 \times 10^{-10}$	0.97	$3.90 \times 10^7$	$4.24 \times 10^{-9}$	0.48	
	21	$8.29 \times 10^6$	$1.83 \times 10^{-10}$	0.97	$1.86 \times 10^7$	$7.87 \times 10^{-8}$	0.24	$7.87 \times 10^{-8}$
	28	$2.48 \times 10^6$	$2.14 \times 10^{-10}$	0.97	$1.68 \times 10^7$	$1.47 \times 10^{-7}$	0.28	$1.10 \times 10^{-8}$
	35	$1.29 \times 10^6$	$2.64 \times 10^{-10}$	0.96	$3.81 \times 10^6$	$1.65 \times 10^{-7}$	0.35	$1.98 \times 10^{-7}$
GA-LDH/EP	7	$1.10 \times 10^9$	$4.88 \times 10^{-11}$	0.97	$4.00 \times 10^9$	$2.12 \times 10^{-10}$	0.49	
	14	$3.29 \times 10^9$	$2.92 \times 10^{-11}$	0.97	$1.66 \times 10^9$	$1.76 \times 10^{-9}$	0.41	
	21	$4.71 \times 10^8$	$2.82 \times 10^{-11}$	0.97	$1.50 \times 10^9$	$3.70 \times 10^{-9}$	0.63	$3.70 \times 10^{-9}$
	28	$3.38 \times 10^8$	$4.72 \times 10^{-11}$	0.97	$9.57 \times 10^8$	$1.81 \times 10^{-8}$	0.65	$5.85 \times 10^{-9}$
	35	$1.77 \times 10^8$	$3.70 \times 10^{-11}$	0.97	$3.46 \times 10^8$	$1.61 \times 10^{-8}$	0.74	$6.89 \times 10^{-9}$

The NSS test was performed on the prepared coating samples in high humidity and high salinity environments. Figure 11 shows the test results for all samples after 1, 2, 6, 10 and 14 days of exposure, respectively. It can be observed that pure EP, LDH/EP, and GA-LDH/EP show different degrees of corrosion, with a significant accumulation of corrosion products and peeling around the artificially scratched region. However, the pure EP coating peeling area was relatively large, and in 14 days there were two corrosive points, indicating that the corrosion was more serious. In contrast, the addition of LDH and GA-LDH effectively slowed down the corrosion, and the edges of the scratched region only started to blister after 6 days for both sample coatings. The peeled area was significantly reduced after 14 days of exposure compared to the pure EP coating. This was due to a few facts. On the one hand, both fillers can capture corrosive  $\text{Cl}^-$ . On the other hand, the lamellar structure of the filler effectively increased the corrosion channel path and effectively hindered the diffusion of corrosive media. Compared with the LDH/EP coating, the GA-LDH/EP coating had relatively fewer corrosion products in the scratched region and was less likely to peel off. The reason for this phenomenon was that the released GA played an active role in corrosion inhibition. According to the results of the above analysis, the addition of GA-LDH was beneficial for the EP coating to show more excellent performance in the NSS test.

### 3.3. Corrosion Protection Mechanism of the GA-LDH/EP Coating

In summary, Figure 12 presents the protection mechanism of the GA-LDH/EP coating. When the coating is exposed to NaCl solution over an extended period, corrosive  $\text{Cl}^-$ ,  $\text{H}_2\text{O}$ , and  $\text{O}_2$  penetrate the coating through micro-pores and micro-cracks to form corrosion channels. In contrast, the addition of GA-LDH has a laminar structure that effectively prolongs corrosion channels and delays the onset of corrosion. When the GA-LDH filler comes into contact with the  $\text{Cl}^-$  that penetrates the coating and traps it, an anion exchange reaction occurs to release gallate anions to maintain a charge balance. At the same time, the released gallate anion can act as a chelating agent to chelate with  $\text{Fe}^{2+}$  and  $\text{Fe}^{3+}$  through

the *o*-phenolic hydroxyl group to form Fe–O–C bonds. The chelate formed with Fe<sup>2+</sup> will be gradually oxidized to the more stable Fe<sup>3+</sup> chelate [54]. The resulting chelate improves corrosion resistance and reduces the corrosion rate, and this chelation bonding improves the force of the EP coating on the Q235 steel surface [23,55]. This mechanism explains why GA-LDH can improve the corrosion protection performance of EP coatings.

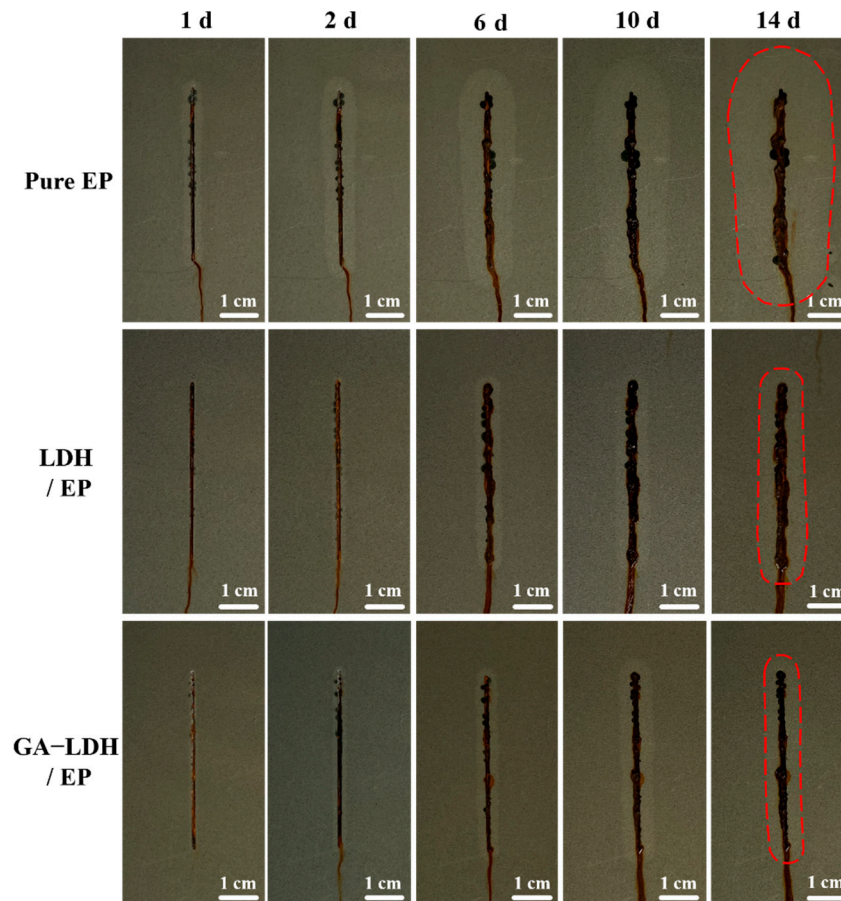


**Figure 11.** Optical photographs of pure EP, LDH/EP, and GA–LDH/EP coatings after neutral salt spray tests at different times. The area where the coating blisters and peels off around the scratched region is plotted by the red dotted line.

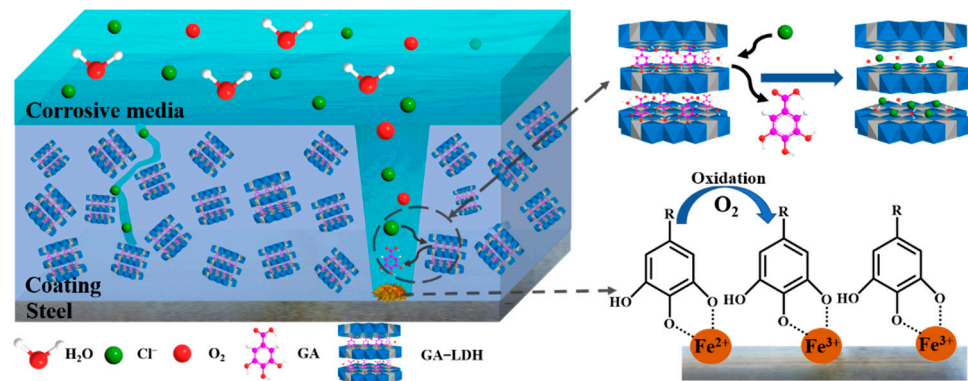


**Figure 12.** Schematic diagram of the corrosion protection mechanism of the GA–LDH/EP coating.

#### 4. Conclusions

In this paper, GA intercalated layered double hydroxide (GA-LDH) was successfully synthesized by the co-precipitation method and was added to epoxy coatings as filler to

improve the corrosion protection performance. According to the XRD results, the layer spacing of GA-LDH samples increased to 1.26 nm, which successfully confirms the gallate anion embedding in LDH. Meanwhile, the UV-vis test confirms that gallate anion can be gradually released in solution with corrosive chloride ions. In addition, GA-LDH/EP performed well at all stages of the electrochemical testing process. The addition of GA-LDH greatly improved the impedance value of the EP coating, dropping by only one order of magnitude in 35 days of immersion. In the neutral salt spray test, the GA-LDH/EP shows fewer corrosion products at the scratches and less peeling area around the scratches. In short, GA-LDH plays an active and protective role as an environmentally friendly corrosion protection filler. The lamellar structure hinders the diffusion of corrosive media, while GA-LDH captures corrosive  $\text{Cl}^-$  and releases gallate anions as chelating agents, effectively protecting metal substrates.

**Author Contributions:** Conceptualization, N.W. and K.C.; Methodology, K.C.; Software, L.W.; Formal analysis, Y.W.; Investigation, S.F. and Y.C.; Resources, S.G.; Data curation, S.F. and Y.C.; Writing—original draft preparation, S.F. and H.Y.; Writing—review and editing, H.Y.; Visualization, Y.W.; Supervision, S.Y.; Project administration, K.C.; Funding acquisition, Y.C. and N.W. All authors have read and agreed to the published version of the manuscript.

**Funding:** This work was supported by the “Jie Bang Gua Shuai” of Science and Technology Projects of Liaoning Province in 2021, grant number 2021JH1/10400091; State Key Laboratory for Marine Corrosion and Protection Foundation, grant number JS220902; Sino-Spain Joint Laboratory on Material Science, grant number 2022JH2/10700005; Shenyang Science and Technology Program-Major Key Core Technology Project, grant number 20-202-1-15; and Liao Ning Revitalization Talents Program, grant number XLYC2005002.

**Institutional Review Board Statement:** Not applicable.

**Informed Consent Statement:** Not applicable.

**Data Availability Statement:** Not applicable.

**Conflicts of Interest:** The authors declare no conflict of interest.

## References

1. Zhao, X.; Yuan, S.; Jin, Z.; Zhu, Q.; Zheng, M.; Jiang, Q.; Song, H.; Duan, J. Fabrication of composite coatings with core-shell nanofibers and their mechanical properties, anticorrosive performance, and mechanism in seawater. *Prog. Org. Coat.* **2020**, *149*, 105893.
2. Nayak, S.R.; Mohana, K.N.S.; Hegde, M.B.; Rajitha, K.; Madhusudhana, A.M.; Naik, S.R. Functionalized multi-walled carbon nanotube/polyindole incorporated epoxy: An effective anti-corrosion coating material for mild steel. *J. Alloys Compd.* **2021**, *856*, 158057. [[CrossRef](#)]
3. Cheng, M.; Li, F.; Wang, Z.; Li, C.; Sun, S.; Hu, S. New valve-free organosilica nanocontainer for active anticorrosion of polymer coatings. *Compos. B Eng.* **2021**, *224*, 109185.
4. Xue, D.; Meng, Q.B.; Lu, Y.X.; Liang, L.; Wei, Y.H.; Liu, X.B. Achieving high performance anticorrosive coating via in situ polymerization of polyurethane and poly(propylene oxide) grafted graphene oxide composites. *Corros. Sci.* **2020**, *176*, 109055.
5. Aghili, M.; Yazdi, M.K.; Ranjbar, Z.; Jafari, S.H. Anticorrosion performance of electro-deposited epoxy/ amine functionalized graphene oxide nanocomposite coatings. *Corros. Sci.* **2021**, *179*, 109143. [[CrossRef](#)]
6. Kang, Y.T.; Wang, C.C.; Chen, C.Y. Corrosion-protective performance of magnetic  $\text{CoFe}_2\text{O}_4$ /polyaniline nanocomposite within epoxy coatings. *J. Taiwan Inst. Chem. Eng.* **2021**, *127*, 357–366.
7. Cao, K.; Yu, Z.; Yin, D.; Chen, L.; Jiang, Y.; Zhu, L. Fabrication of BTA-MOF-TEOS-GO nanocomposite to endow coating systems with active inhibition and durable anticorrosion performances. *Prog. Org. Coat.* **2020**, *143*, 105629. [[CrossRef](#)]
8. Wang, X.; Li, Y.; Li, C.; Zhang, X.; Lin, D.; Xu, F.; Zhu, Y.; Wang, H.; Gong, J.; Wang, T. Highly orientated graphene/epoxy coating with exceptional anti-corrosion performance for harsh oxygen environments. *Corros. Sci.* **2020**, *176*, 109049.
9. AhadiParsa, M.; Dehghani, A.; Ramezanzadeh, M.; Ramezanzadeh, B. Rising of MXenes: Novel 2D-functionalized nanomaterials as a new milestone in corrosion science—a critical review. *Adv. Colloid Interface Sci.* **2022**, *307*, 102730.
10. Wang, G.; Huang, D.; Cheng, M.; Chen, S.; Zhang, G.; Lei, L.; Chen, Y.; Du, L.; Li, R.; Liu, Y. Metal-organic frameworks template-directed growth of layered double hydroxides: A fantastic conversion of functional materials. *Coord. Chem. Rev.* **2022**, *460*, 214467. [[CrossRef](#)]
11. Wang, J.; Qi, Y.; Zhao, X.; Zhang, Z. Electrochemical investigation of corrosion behavior of epoxy modified silicate zinc-rich coatings in 3.5% NaCl solution. *Coatings* **2020**, *10*, 444. [[CrossRef](#)]

12. Maranescu, B.; Lupa, L.; Mihali, M.T.L.; Plesu, N.; Maranescu, V.; Visa, A. The corrosion inhibitor behavior of iron in saline solution by the action of magnesium carboxyphosphonate. *Pure Appl. Chem.* **2018**, *90*, 1713–1722. [[CrossRef](#)]
13. Pourhashem, S.; Saba, F.; Duan, J.; Rashidi, A.; Guan, F.; Nezhad, E.G.; Hou, B. Polymer/Inorganic nanocomposite coatings with superior corrosion protection performance: A review. *J. Ind. Eng. Chem.* **2020**, *88*, 29–57.
14. Su, Y.; Qiu, S.; Yang, D.; Liu, S.; Zhao, H.; Wang, L.; Xue, Q. Active anti-corrosion of epoxy coating by nitrite ions intercalated MgAl LDH. *J. Hazard. Mater.* **2020**, *391*, 122215. [[CrossRef](#)]
15. Tabish, M.; Yasin, G.; Anjum, M.J.; Malik, M.U.; Zhao, J.; Yang, Q.; Manzoor, S.; Murtaza, H.; Khan, W.Q. Reviewing the current status of layered double hydroxide-based smart nanocontainers for corrosion inhibiting applications. *J. Mater. Res. Technol.* **2021**, *10*, 390–421.
16. Li, W.; Liu, A.; Tian, H.; Wang, D. Controlled release of nitrate and molybdate intercalated in Zn-Al-layered double hydroxide nanocontainers towards marine anticorrosion applications. *Colloid. Interface Sci. Commun.* **2018**, *24*, 18–23. [[CrossRef](#)]
17. Wang, N.; Gao, H.; Zhang, J.; Li, L.; Fan, X.; Diao, X. Anticorrosive waterborne epoxy (EP) coatings based on sodium tripolyphosphate-pillared layered double hydroxides (STPP-LDHs). *Prog. Org. Coat.* **2019**, *135*, 74–81. [[CrossRef](#)]
18. Liu, A.; Tian, H.; Li, W.; Wang, W.; Gao, X.; Han, P.; Ding, R. Delamination and self-assembly of layered double hydroxides for enhanced loading capacity and corrosion protection performance. *Appl. Surf. Sci.* **2018**, *462*, 175–186. [[CrossRef](#)]
19. Alibakhshi, E.; Ghasemi, E.; Mahdavian, M.; Ramezanzadeh, B.; Farashi, S. Active corrosion protection of Mg-Al-PO<sub>4</sub><sup>3-</sup> LDH nanoparticle in silane primer coated with epoxy on mild steel. *J. Taiwan. Inst. Chem. Eng.* **2017**, *75*, 248–262. [[CrossRef](#)]
20. Qu, W.; Breksa, I.A.P.; Pan, Z.; Ma, H. Quantitative determination of major polyphenol constituents in pomegranate products. *Food Chem.* **2012**, *3*, 1585–1591. [[CrossRef](#)]
21. Damiani, E.; Bacchetti, T.; Padella, L.; Tiano, L.; Carloni, P. Antioxidant activity of different white teas: Comparison of hot and cold tea infusions. *J. Food Compos. Anal.* **2014**, *33*, 59–66. [[CrossRef](#)]
22. Tako, E.; Beebe, S.E.; Reed, S.; Hart, J.J.; Glahn, R.P. Polyphenolic compounds appear to limit the nutritional benefit of biofortified higher iron black bean (*Phaseolus vulgaris* L.). *Nutr. J.* **2014**, *13*, 28. [[CrossRef](#)] [[PubMed](#)]
23. Li, J.; Ge, S.; Wang, J.; Du, H.; Song, K.; Fei, Z.; Shao, Q.; Guo, Z. Water-based rust converter and its polymer composites for surface anticorrosion. *Colloids Surf. A Physicochem. Eng. Asp.* **2018**, *537*, 334–342.
24. Lei, Y.; Yu, P.; Peng, H.; Luan, Z.; Deng, S.; Wang, S.; Zhou, N. Water-based & eco-friendly & high-efficiency 3,4,5-Trihydroxybenzoic acid ester as a novel rust conversion agent and its polymer composites for enhanced surface anticorrosion. *Colloids Surf. A Physicochem. Eng. Asp.* **2021**, *626*, 127065.
25. Pérez-Almeida, N.; González, A.G.; Santana-Casiano, J.M.; González-Dávila, M. Ocean acidification effect on the iron-gallic acid redox interaction in seawater. *Front. Mar. Sci.* **2022**, *9*, 837363.
26. Rodriguez, J.; Bollen, E.; Nguyen, T.D.; Portier, A.; Paint, Y.; Olivier, M.G. Incorporation of layered double hydroxides modified with benzotriazole into an epoxy resin for the corrosion protection of Zn-Mg coated steel. *Prog. Org. Coat.* **2020**, *149*, 105894. [[CrossRef](#)]
27. Cao, Y.; Zheng, D.; Zhang, F.; Pan, J.; Lin, C. Layered double hydroxide (LDH) for multi-functionalized corrosion protection of metals: A review. *J. Mater. Sci. Technol.* **2022**, *102*, 232–263.
28. Zou, K.; Zhang, H.; Duan, X. Studies on the formation of 5-aminosalicylate intercalated Zn-Al layered double hydroxides as a function of Zn/Al molar ratios and synthesis routes. *Chem. Eng. Sci.* **2007**, *62*, 2022–2031. [[CrossRef](#)]
29. Lou, C.; Zhang, R.; Lu, X.; Zhou, C.; Xin, Z. Facile fabrication of epoxy/polybenzoxazine based superhydrophobic coating with enhanced corrosion resistance and high thermal stability. *Colloids Surf. A* **2019**, *562*, 8–15. [[CrossRef](#)]
30. He, J.; Li, M.; Li, D.; Bao, B.; Xue, M.; Huang, Y.; Xu, Y.; Chen, G.; Dai, L. Fabrication of azobenzene non-covalent bonding grafting graphene composite and its application in weathering and corrosion resistant polyurethane coating. *Polym. Degrad. Stab.* **2022**, *206*, 110157. [[CrossRef](#)]
31. Alibakhshi, E.; Ghasemi, E.; Mahdavian, M.; Ramezanzadeh, B.; Mana, y. The effect of interlayer spacing on the inhibitor release capability of layered double hydroxide based nanocontainers. *J. Clean. Prod.* **2020**, *251*, 119676. [[CrossRef](#)]
32. Kleyi, P.E.; Mudaly, P.; Pillai, S.K.; de Beer, M. Zn/Al Layered double hydroxides nanostructure as effective controlled release vehicle of nicotinic acid for topical applications. *Appl. Clay Sci.* **2021**, *215*, 106304. [[CrossRef](#)]
33. Iyi, N.; Yamada, H.; Sasaki, T. Deintercalation of carbonate ions from carbonate-type layered double hydroxides (LDHs) using acid-alcohol mixed solutions. *Appl. Clay Sci.* **2011**, *54*, 132–137. [[CrossRef](#)]
34. Salak, A.N.; Tedim, J.; Kuznetsova, A.I.; Ribeiro, J.L.; Vieira, L.G.; Zheludkevich, M.L. Ferreira MGS. Comparative X-ray diffraction and infrared spectroscopy study of Zn-Al layered double hydroxides: Vanadate vs nitrate. *Chem. Phys.* **2012**, *397*, 102–108. [[CrossRef](#)]
35. Shamim, M.; Dana, K. Intercalation of LDH NO<sub>3</sub> with short-chain intercalants. *Bull. Mater. Sci.* **2019**, *42*, 25. [[CrossRef](#)]
36. Cao, Y.; Zheng, D.; Dong, S.; Zhang, F.; Lin, J.; Wang, C.; Lin, C. A composite corrosion inhibitor of MgAl Layered double hydroxides co-intercalated with hydroxide and organic anions for carbon steel in simulated carbonated concrete pore solutions. *J. Electrochem. Soc.* **2019**, *166*, C3106–C3113. [[CrossRef](#)]
37. Ma, L.; Qiang, Y.; Zhao, W. Designing novel organic inhibitor loaded MgAl-LDHs nanocontainer for enhanced corrosion resistance. *Chem. Eng. J.* **2021**, *408*, 127367. [[CrossRef](#)]
38. Wang, Y.; Zhang, D. Synthesis, characterization, and controlled release anticorrosion behavior of benzoate intercalated Zn-Al layered double hydroxides. *Mater. Res. Bull.* **2011**, *46*, 1963–1968. [[CrossRef](#)]

39. Ruiz, C.V.; Rodríguez-Castellón, E.; Giraldo, O. Hybrid materials based on a layered zinc hydroxide solid and gallic acid: Structural characterization and evaluation of the controlled release behavior as a function of the gallic acid content. *Appl. Clay Sci.* **2019**, *181*, 105228. [[CrossRef](#)]
40. Kong, X.; Jin, L.; Wei, M.; Duan, X. Antioxidant drugs intercalated into layered double hydroxide: Structure and in vitro release. *Appl. Clay Sci.* **2010**, *49*, 324–329. [[CrossRef](#)]
41. Lu, S.; Liu, L.; Wang, H.; Zhao, W.; Li, Z.; Qu, Z.; Li, J.; Sun, T.; Wang, T.; Sui, G. Synthesis of dual functional gallic-acid-based carbon dots for bioimaging and antitumor therapy. *Biomater. Sci.* **2019**, *7*, 3258–3265. [[CrossRef](#)]
42. Barr, T.L.; Seal, S. Nature of the use of adventitious carbon as a binding energy standard. *J. Vac. Sci. Technol. A* **1995**, *13*, 1239–1246. [[CrossRef](#)]
43. Cao, Y.; Jin, S.; Zheng, D.; Lin, C. Facile fabrication of ZnAl layered double hydroxide film co-intercalated with vanadates and laurates by one-step post modification. *Colloids Interface Sci.* **2021**, *40*, 100351. [[CrossRef](#)]
44. Toth, I.Y.; Szekeres, M.; Turcu, R.; Saringer, S.; Illes, E.; Nesztor, D.; Tombacz, E. Mechanism of in situ surface polymerization of gallic acid in an environmental-inspired preparation of carboxylated core-shell magnetite nanoparticles. *Langmuir* **2014**, *30*, 15451–15461. [[CrossRef](#)]
45. Theiss, F.L.; Ayoko, G.A.; Frost, R.L. Thermogravimetric analysis of selected layered double hydroxides. *J. Therm. Anal. Calorim.* **2012**, *112*, 649–657. [[CrossRef](#)]
46. Starukh, G.; Rozovik, O.; Oranska, O. Organo/Zn-Al LDH nanocomposites for cationic dye removal from aqueous media. *Nanoscale Res. Lett.* **2016**, *11*, 228. [[CrossRef](#)]
47. Karami, Z.; Jouyandeh, M.; Ali, J.A.; Ganjali, M.R.; Aghazadeh, M.; Paran, S.M.R.; Naderi, G.; Puglia, D.; Saeb, M.R. Epoxy/layered double hydroxide (LDH) nanocomposites: Synthesis, characterization, and Excellent cure feature of nitrate anion intercalated Zn-Al LDH. *Prog. Org. Coat.* **2019**, *136*, 105218. [[CrossRef](#)]
48. Hafez, I.H.; Osman, A.R.; Sewedan, E.A.; Berber, M.R. Tailoring of a potential nanoformulated form of gibberellic acid: Synthesis, characterization, and field applications on vegetation and flowering. *J. Agric. Food Chem.* **2018**, *66*, 8237–8245. [[CrossRef](#)]
49. Ghotbi, M.Y.; bin Hussein, M.Z. Gallate-Zn-Al-layered double hydroxide as an intercalated compound with new controlled release formulation of anticarcinogenic agent. *J. Phys. Chem. Solids* **2010**, *71*, 1565–1570. [[CrossRef](#)]
50. Shen, L.; Li, Y.; Zhao, W.; Wang, K.; Ci, X.; Wu, Y.; Liu, G.; Liu, C.; Fang, Z. Tuning F-doped degree of rGO: Restraining corrosion-promotion activity of EP/rGO nanocomposite coating. *J. Mater. Sci. Technol.* **2020**, *44*, 121–132. [[CrossRef](#)]
51. Wang, N.; Diao, X.; Zhang, J.; Kang, P. Corrosion Resistance of waterborne epoxy coatings by incorporation of dopamine treated mesoporous-TiO<sub>2</sub> particles. *Coatings* **2018**, *8*, 209. [[CrossRef](#)]
52. Xu, J.; Gao, F.; Wang, H.; Dai, R.; Dong, S.; Wang, H. Organic/inorganic hybrid waterborne polyurethane coatings with self-healing properties for anticorrosion application. *Prog. Org. Coat.* **2023**, *174*, 107244. [[CrossRef](#)]
53. Qiang, Y.; Zhang, S.; Guo, L.; Zheng, X.; Xiang, B.; Chen, S. Experimental and theoretical studies of four allyl imidazolium-based ionic liquids as green inhibitors for copper corrosion in sulfuric acid. *Corros. Sci.* **2017**, *119*, 68–78. [[CrossRef](#)]
54. Wang, X.; Zhu, Q.; Liu, X.; Hou, B. Rust conversion performance of phosphoric acid-gallic acid in vinyl chloride acrylic emulsion. *Coatings* **2021**, *11*, 152. [[CrossRef](#)]
55. Jia, Y.; Ren, N.; Yue, H.; Deng, J.; Liu, Y. Preparation and properties of natural gallic acid based rust conversion emulsion. *Pigm. Resin. Technol.* **2016**, *45*, 191–198. [[CrossRef](#)]

**Disclaimer/Publisher’s Note:** The statements, opinions and data contained in all publications are solely those of the individual author(s) and contributor(s) and not of MDPI and/or the editor(s). MDPI and/or the editor(s) disclaim responsibility for any injury to people or property resulting from any ideas, methods, instructions or products referred to in the content.